Clinical translation of ultrasoft Fleuron™ probes for stable, high-density, and bidirectional brain interfaces

Jongha Lee[a], Hyunsu Park[a], Andrew Spencer[a], Xian Gong[a], Matt DeNardo[a], Foad Vashahi[a], Florent Pollet[a], Samantha Norris[a], Henry Hinton[a], Méliya El Fakiri[a], Anant Mehrotra[a], Rongchen Huang[a], Julian Bär[a], Jake Swann[a], Dave Affonseca Jr.[a], Oliver Armitage[a], Ryan Garry[a], Emily Grumbles[a], Akash Murali[a], Jordy Tasserie[a], Caua Fragoso[a], Romain Albouy[a], Charles P. Couturier[a,c], Angelique C. Paulk[d], Brian Coughlin[d], Sydney S. Cash[d], Beth Costine-Bartell[e], Benjamin Baskin[e], Tawny Stinson[e], Homeira Moradi Chameh[f], Mandana Movahed[f], Bamdad Bazrgar[g], Madeleine Falby[g], Darren Zhang[h], Taufik A. Valiante[f, i], Ariel Francis[j], Carlos Candanedo[j], Ricardo Bermúdez[j], Jia Liu[a,b], Tianyang Ye[a,*], Paul Le Floch [a,*]

[a] Axoft, Inc., Cambridge, MA, USA.
[b] John A. Paulson School of Engineering and Applied Sciences, Harvard University, Boston, MA, USA
[c] Montreal Neurological Institute-Hospital, Montreal, QC, Canada; Department of Neurology and Neurosurgery, McGill University, Montreal, QC, Canada; Department of Human Genetics, McGill University, Montreal, QC, Canada; Broad Institute of MIT and Harvard, Cambridge, MA, USA; Institute for Medical Engineering and Sciences, Massachusetts Institute of Technology, Cambridge, MA, USA; Department of Neurosurgery, Brigham and Women's Hospital, Mass General Brigham, Boston, MA, USA
[d] Mass General Hospital, Center for Neurotechnology and Neurorecovery, Department of Neurology, Harvard Medical School, Boston, MA
[e] MGH Brain Trauma Lab, Department of Neurosurgery, Massachusetts General Hospital, Harvard Medical School, Boston, MA
[f] Division of Clinical and Computational Neuroscience, Krembil Brain Institute, University Health Network (UHN), Toronto, CA
[g] Institute of Medical Science, University of Toronto, Toronto, CA
[h] Department of Physiology and Pharmacology, Medical Sciences, University of Western Ontario, London, CA
[i] Institute of Medical Science, University of Toronto, Toronto, ON, Canada; Institute of Biomedical Engineering, University of Toronto, Toronto, ON, Canada; Department of Electrical and Computer Engineering, University of Toronto, Toronto, ON, Canada; Division of Neurosurgery, Department of Surgery, University of Toronto, Toronto, ON, Canada; Center for Advancing Neurotechnological Innovation to Application (CRANIA), Toronto, ON, Canada; Max Planck-University of Toronto Center for Neural Science and Technology, University of Toronto, Toronto, ON, Canada
[j] The Panama Clinic, Panama City, Panama
*Correspondence should be addressed to info@axoft.us

Building brain foundation models to capture the underpinning neural dynamics of human behavior requires large functional neural datasets for training, which current implantable Brain-Computer Interfaces (iBCIs) cannot obtain due to the instability of rigid materials in the brain. How can we achieve high-density neural recordings with wide brain region access at single-neuron resolution, while maintaining long-term stability? In this study, we present a novel approach to overcome these trade-offs by introducing Fleuron, a family of ultrasoft, ultra-low-k dielectric materials compatible with thin-film scalable microfabrication techniques. We successfully integrate up to 1,024 channels within a single minimally invasive Fleuron depth electrode. The combination of the novel implant material and geometry enables single-unit level recordings for 18 months in rodent models, and achieves a large number of units detected per electrode across animals. 128-channel Fleuron probes, that cover 8× larger tissue volume than state-of-the-art polyimide counterparts, can track over 100 single-units over months. Stability in neural recordings correlates with reduced glial encapsulation compared to polyimide controls up to 9-month post-implantation. Fleuron probes are integrated with a low-power, mixed-signal ASIC to achieve over 1,000 channels electronic interfaces and can be safely implanted in depth using minimally invasive surgical techniques via a burr hole approach without requiring specialized robotics. Fleuron probes further create a unique contrast in clinical 3T MRI, allowing for post-operative position confirmation. Large-animal and *ex vivo* human tissue studies confirm safety and functionality in larger brains. Finally, Fleuron probes are used for the first time ever intraoperatively during planned resection surgeries, confirming in-human usability, and demonstrating the potential of the technology for clinical translation in iBCIs.

Introduction

Over 40% of the world's population suffers from some form of neurological disorder (1), many of which lack effective treatments or cures, severely impacting the quality of life for billions of individuals worldwide. In these cases, implantable Brain-Computer Interfaces (iBCIs) offer significant promise due to their unique ability to decode patient intentions, restore functional capabilities (2, 3), and facilitate personalized therapies by identifying novel biomarkers of neurological diseases. However, to realize widespread adoption, iBCIs must leverage modern artificial intelligence (AI) models to interpret the underpinning dynamics of brain activity involved during behaviors, thoughts, and across patient populations.

However, large AI models typically require immense volumes (*e.g.* billions of data points) of high-quality data for effective training, exceeding by far what wearable technologies and low-resolution iBCIs such as electrocorticography (ECoG) grids and endovascular sensors can currently provide. Recent preclinical studies employing research-grade microelectrode technologies (4) have demonstrated that AI Foundation Models of the brain can be successfully developed using high-density electrophysiological recordings (5, 6). Nonetheless, existing neural interface technologies face significant challenges in clinical translation, primarily due to inherent limitations associated with rigid implant materials. These challenges include (*i*) the trade-off between achieving high bandwidth – often requiring larger probe footprint to support more recording and stimulation channels – while ensuring chronic stability, which is compromised by glial encapsulation (7) and implant micromotion; (*ii*) invasiveness of surgical implantation, which limits clinical usability, and (*iii*) restricted access to deep brain regions critically involved in many neurological disorders (8).

The stability of the brain-electronics interface fundamentally determines the quality of neural data acquired by iBCIs. Downstream processing alone cannot reliably reconstruct latent neural population dynamics from unstable large-scale

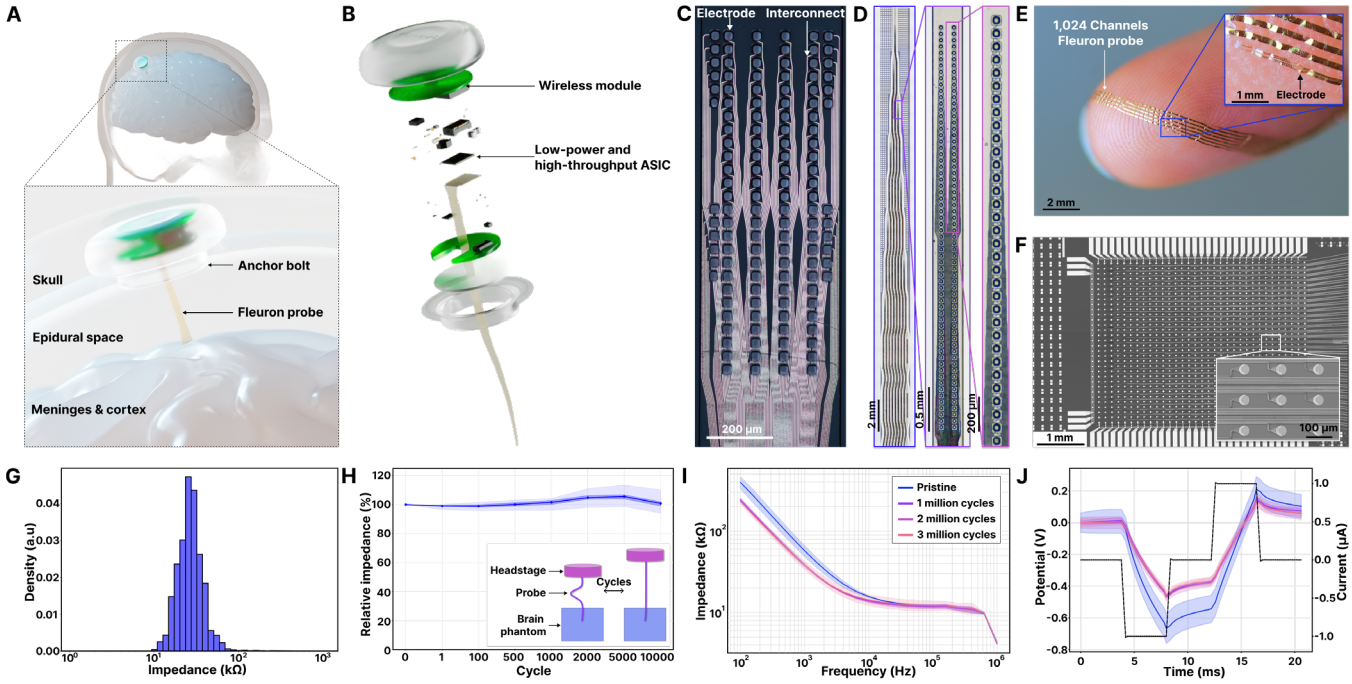

Figure 1. Brain-Computer Interface using Fleuron probes.
(A) Schematic showing the components of an iBCI using an ultrasoft Fleuron probe. **(B)** Exploded view of (A). **(C)** Stitched bright-field microscopic image of a multi-layer and high-density Fleuron probe with 128 channels and **(D)** 1,024 channels. **(E)** The 1024-channel Fleuron probe placed on a fingertip. Inset shows a magnified view of a region with a high-density of sensors/stimulators. **(F)** Microscope image of the 1024-channel Fleuron probe bonding region to an ASIC with high-density I/O pads. Inset provides a scanning electron microscope (SEM) image of contact pads and interconnect lines **(G)** Distribution of electrode impedance @ 1kHz from 128-channel probes obtained from 10 wafers. **(H)** Normalized impedance distribution for each channel, referenced to the initial value at cycle 0, as a function of the number of bending cycles under a 2 mm bending diameter. Color code: Line = mean; dark blue area = 25th to 75th interquartile range; light blue area = min. to max. values. **(I)** Electrochemical impedance spectroscopy (EIS) characterization and **(J)** Voltage transient (VT) measurement of pristine device, and after 1-, 2- and 3- million stimulation cycles. Color code: Line = mean; dark area = 25th to 75th interquartile range; light area = min. to max. values.

single- and multi-unit recordings. Yet, capturing these dynamics is essential for decoding brain activity during behavior across diverse patient populations, particularly given intrinsic sources of signal variability such as representational drift (9). State-of-the-art brain-electronics interfaces utilize rigid materials such as silicon and polyimide (10), originally developed for industrial applications rather than optimized for chronic neural integration. This inherent mechanical mismatch imposes significant, yet avoidable, limitations on the scalability and clinical translation of iBCIs.

Here, we address these challenges by introducing a new class of ultrasoft iBCI material: Fleuron. Fleuron polymers mimic more closely the mechanical properties of brain tissues (Young's modulus ≈ 5 MPa), are compatible with scalable microfabrication, biocompatible and bio-stable, and ultra-low-k (ε = 2.1) thin-film passivation for high-density microelectrode arrays (11, 12). Due to their inherent softness, Fleuron probes maintain stable single-unit resolution despite lateral dimensions eight times larger than those of conventional rigid polyimide probes, effectively minimizing the immune response typically associated with increased probe size. We present various fabricated designs capable of integrating hundreds of sensors and stimulators onto a single implantable thread. Long-term studies demonstrate minimal glial encapsulation around Fleuron probes compared to polyimide controls at 3, 6, and 9 months post-implantation, with stable single-unit recordings maintained for at least 18 months. Chronic recordings using 128-channel Fleuron probes across multiple animals reveal consistently high unit yields and stable performance without significant degradation over more than 6 months. A minimally invasive surgical procedure using an 11 mm (inner diameter) burr hole is presented and Fleuron probes are shown to be visible post-implantation under clinical 3T MRI following implantation at an intended depth without requiring specialized robotics. Acute trials in porcine models confirm the capability of Fleuron probes to record both single- and multi-unit neural activity, while an ovine model demonstrates an absence of glial encapsulation after two weeks of implantation. Finally, we demonstrate the feasibility of using Fleuron probes intraoperatively in humans to establish high-density single-unit resolution recordings and detect neural responses to a local-global deviant auditory paradigm in both anesthetized and awake patients.

Integration of Fleuron Probes in an iBCI

Clinical applications of iBCIs require integration of multiple technologies such as implantable and hermetic electronics, wireless power and data transmission capabilities, and high-throughput interface to sensors. In this work, we show the integration of Fleuron probes to high-throughput application-specific integrated circuit (ASIC) technology supporting multiplexed amplification and analog-to-digital conversion (ADC) for scaling to multiple thousands of recording and

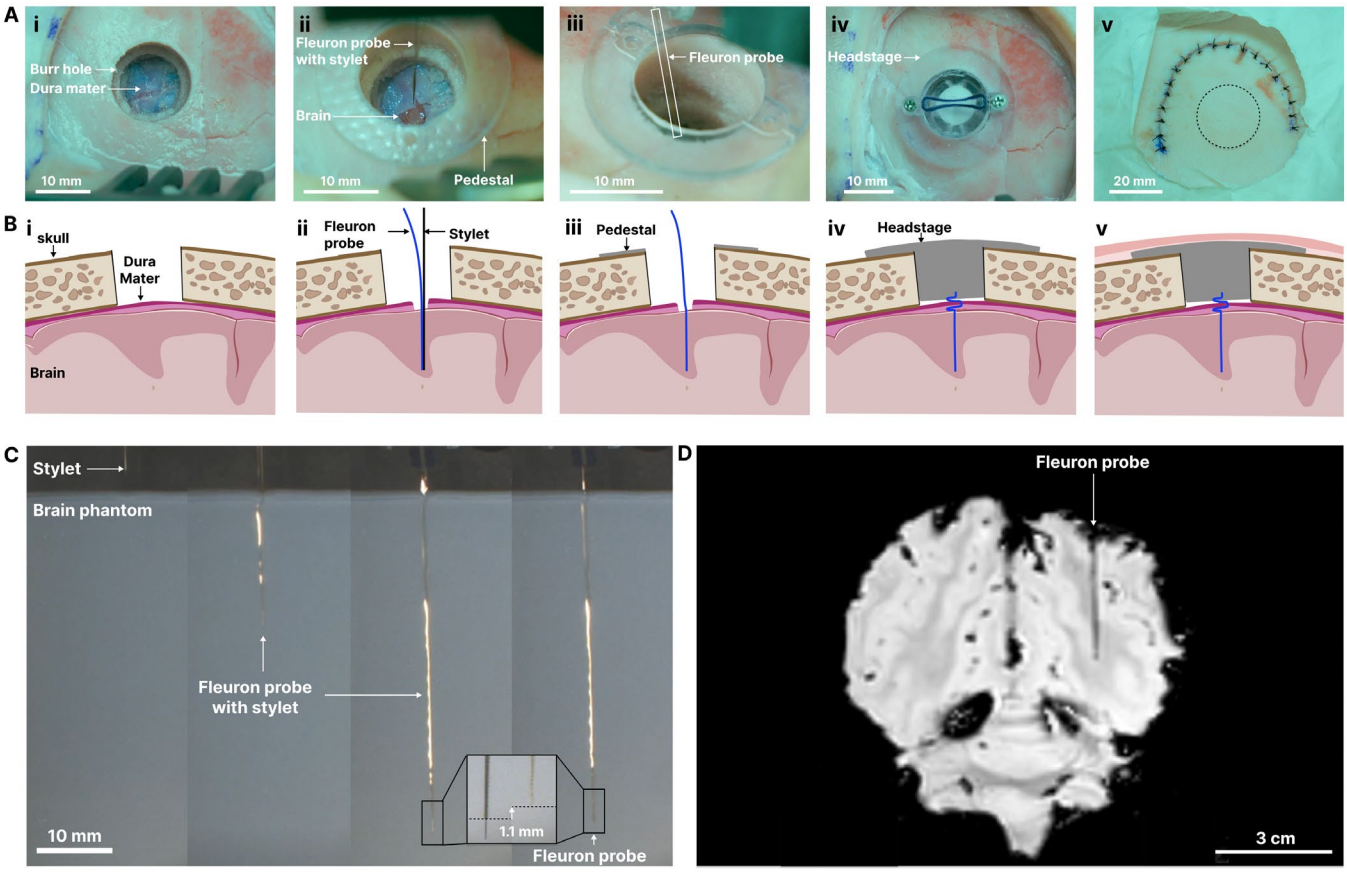

Figure 2 Minimally invasive implantation and imaging of a Fleuron probe for Brain-Computer Interfaces. **(A)** Optical images showing the steps of the minimally invasive implantation procedure of a Fleuron Brain-Computer Interface in an *ex vivo* porcine brain. A standard 14 mm outer diameter and 11 mm inner diameter burr hole is used to access the dura mater. (*i*) Exposed dura mater following burr hole drilling. (*ii*) Implantation of the Fleuron using a stylet after durotomy. (*iii*) Fleuron probe inside brain tissues after the removal of the stylet. (*iv*) Placement of the headstage inside the minimally invasive burr hole. (*v*) Closed surgical site with sutures. **(B)** Corresponding side-view schematic representation of each stage in surgical procedure. **(C)** Optical images of the Fleuron probe with stylet being inserted in a brain phantom (0.6% agarose gel) at 45 mm of depth. Inset shows a magnified view of the probe before and after the retraction of the stylet. **(D)** Magnetic Resonance Imaging (MRI) of the *ex vivo* porcine brain post-implantation.

stimulation channels in a proposed implant configuration compatible with minimally invasive burr-hole surgery (**Fig. 1A, B).** Current Fleuron probes can support 128 to 1,024 recording/stimulation channels per thread (**Fig. 1C, D**), where electrode sites' position and density can be tailored depending on the targeted brain region and implantation depth, due to the compatibility of Fleuron with standard mask- and maskless photo-patterning techniques. Standard metal (Pt, Au, Ti) and metal-oxide (IrO_x, TiN) frameworks can be used to realize high-density interconnects (5-µm pitch) and low-impedance sites. We design a high-throughput I/O interface connecting Fleuron-encapsulated traces to standard substrates (*e.g.* Si, SiO_2, Glass), and flip-chip bonded to an ultra-high channel count ASIC (**Fig. 1E, F**), allowing multiplexed neural recording and stimulation from each electrode site.

Electrochemical and Mechanical Performances

Impedance of 32 µm diameter platinum black-coated electrodes (**Fig. 1G**) across a batch of 10 wafers shows a unimodal distribution with an average impedance value of 39.6 ± 8.0 kΩ at 1kHz across the entire electrode array, showing the reliability of the multilayer fabrication process using Fleuron in pre-manufacturing stage.

A major limitation of rigid polyimide implants is the progressive displacement, or "drift", between the probe and surrounding brain tissue over time, driven by the mechanical mismatch and the natural movement of the brain inside the skull. This drift can lead to signal instability, electrical failure, and in severe cases, complete detachment from the implantation site. Fleuron probes inherently mitigate this issue through their extreme mechanical compliance (Young's modulus ≈ 5 MPa vs. ≈ 3,000 MPa for polyimide), allowing the implant to adapt to biomechanical movements. To assess mechanical stability, we performed cyclic bending tests (bending radius of 2 mm) (**Fig. 1H**), which showed no signs of probe displacement inside the brain phantom, and minimal impedance variations across electrodes – within 10% of the initial impedance value after 10,000 cycles. These findings underscore the suitability of Fleuron probes for chronically stable neural recordings.

Additionally, electrodes embedded in Fleuron can also inject small currents. We show that 32-µm diameter Titanium Nitride-coated electrodes can sustain over three million cycles

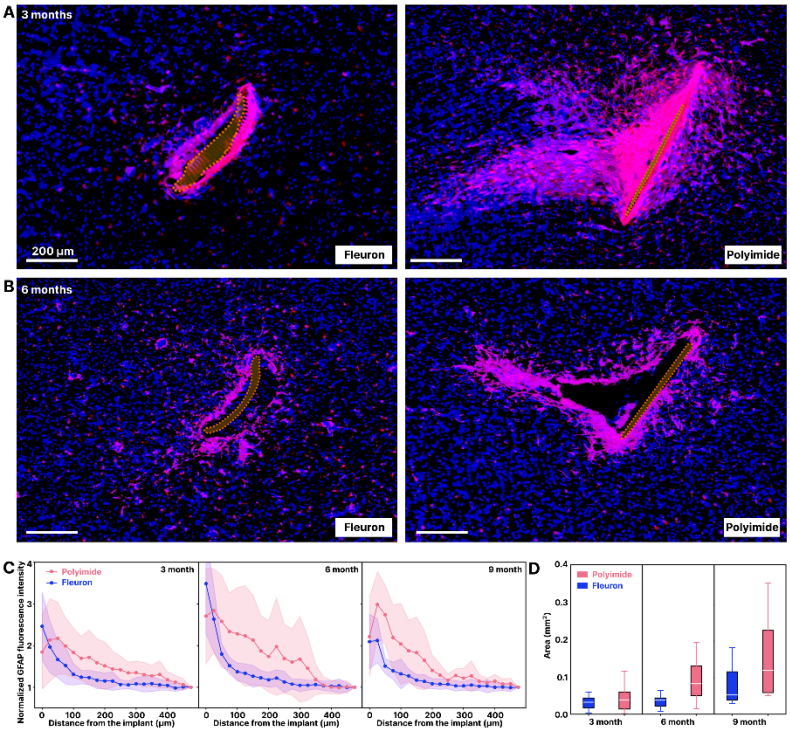

Figure 3 Chronic local tissue response to Fleuron probes versus Polyimide probes. **(A)** Representative immunofluorescence images of horizontal brain tissue sections obtained at 3 months and 6 months following implantation of a Fleuron probe (left) and a polyimide probe (right) in the same rat brain. Staining includes DAPI (blue) for cell nuclei, GFAP (pink) for astrocytes indicating glial scarring, and Iba1 (red) for activated microglia representing neuroinflammatory responses. Probes' cross-sections are colored in orange. Both probes have identical geometries: 10 µm in thickness and 700 µm in width. Each probe is implanted in one hemisphere of the rodent brain. **(B)** Quantitative analysis of normalized GFAP fluorescence intensity as a function of distance from the probe-tissue interface for Fleuron (blue) and polyimide (pink) implants (N=5, 7 and 8 subjects per time point). Lines show the mean value and shaded regions show the standard error of the mean (SEM). **(C)** Normalized average cavity size in rodents at the electrode-tissue interface for both types of probes.

of stimulation (1 mV cathodic pulse followed by an anodic pulse, each lasting 4 ms, with a 4 ms interpulse delay) with minimal variations in electrochemical impedance and voltage transient (**Fig. 1I, 1J**), highlighting the technology's potential for reliable and long-term micro-stimulation applications.

Minimally Invasive Implantation Process

The headstage and the probe can be implanted and secured in a manner comparable to existing minimally invasive neurosurgical procedures, such as implantation of deep brain stimulation (DBS) leads and stereo-electroencephalography (sEEG) electrodes, ensuring its compatibility with established clinical workflows.

Figures 2A and 2B depict the minimally invasive procedure in a porcine brain. After neuronavigation calibration, a small burr hole is made at the implantation site. After durotomy, the Fleuron probe is inserted to the planned depth using a custom 125 µm tungsten stylet, via either a frameless or frame-based approach. Once positioned, the stylet is disengaged and carefully withdrawn. The headstage is then secured to the skull, and the incision is closed. As shown in **Figure 2C**, implantation into a brain phantom demonstrates precise depth targeting with minimal retraction. The third panel shows the probe fully inserted to a depth of 45 mm with the stylet still in place, showcasing the ability to reach subcortical structures for brain-wide access. In panel four, positional shift during stylet retraction is limited to approximately 2%, highlighting the probe's mechanical stability during deployment.

Magnetic Resonance Imaging (MRI)-Visibility

Depth placement of Fleuron probes can be confirmed after removal of the stylet using MRI. **Figure 2D** shows T2-weighted MRI scans at 3 Tesla from a porcine cadaver model, revealing the implanted probe as a distinct ^{1}H signal void. This visibility arises from Fleuron's low protium density and its sufficiently large geometrical dimensions, offering a clear contrast against surrounding brain tissue, unlike conventional hydrocarbon-based microelectrode arrays, like polyimide probes, that typically lack MRI contrast due to their atomic composition and narrow dimensions.

The visibility of Fleuron probes in post-operative MRI enables confirmation of device placement, which is critical when targeting deep cortical and subcortical structures involved in many neurological disorders (13).

Minimized Glial Encapsulation and Tissue Damage Around Larger Probes

State-of-the-art laminar arrays fabricated from conventional rigid materials such as polyimide or silicon often induce significant tissue scarring over time, contributing to signal degradation and instability of neural recordings (7, 14). To minimize gliosis, the dimensions of rigid polyimide probes are typically constrained to widths below 70 µm and thicknesses under 2–5 µm (10). However, these size limitations restrict the integration of high-density sensing and stimulation sites, reduce tissue coverage, increase capacitive leakage, and elevate the risk of mechanical failure, ultimately limiting the scalability and performance of neural interfaces.

In our previous work, we demonstrated that Fleuron probes with cross-sectional dimensions of up to 250 × 10 µm² induced significantly less gliosis than rigid epoxy-based counterparts (SU-8) following up to 12 weeks of implantation (12). In the present study, we further increase the cross-sectional dimensions of both the Fleuron probes and a polyimide control to 700 × 10 µm² and assess chronic local tissue responses using immunofluorescence imaging in a rat model. We use a 125 µm diameter tungsten stylet, a clinically relevant size that enables deep brain implantation while minimizing the risk of deflection during insertion. Horizontal brain slices (**Fig. 3A**) revealed a

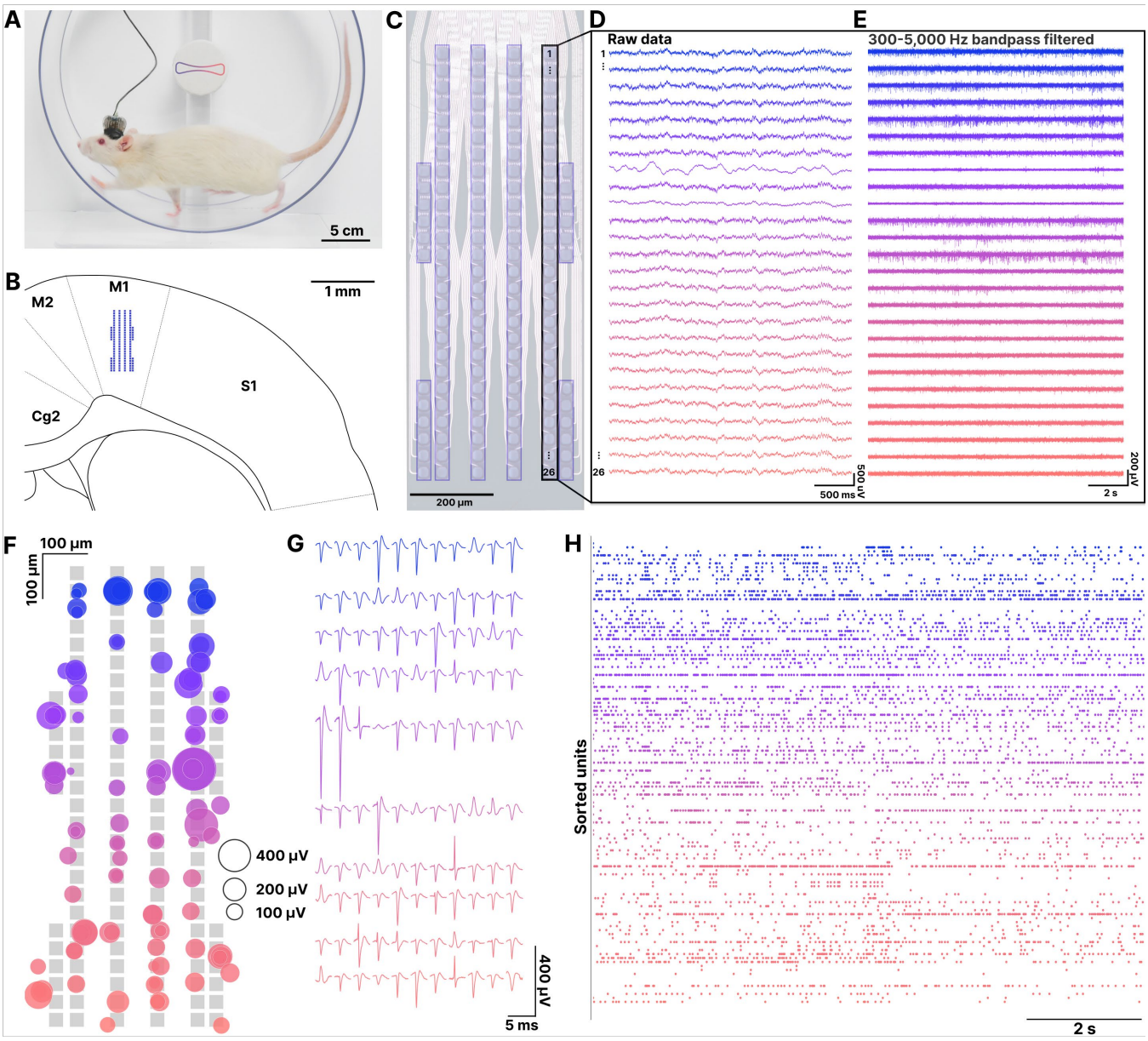

Figure 4. Tissue-wide, high-density single- and multi-unit recordings using Fleuron probes.
(A) Photograph of a rat implanted with a Fleuron probe. **(B)** Schematic illustration of the probe placement within the primary motor cortex (M1). **(C)** Microscopic image of a 128-channel Fleuron probe with 6 columns of electrodes. **(D)** Representative raw, and **(E)** bandpass-filtered (300–5,000 Hz) voltage traces from a single column of electrodes. **(F)** Visualization of spike sorting results using Kilosort 4, showing the spatial distribution (centroid) and relative amplitude of identified units across the electrodes. **(G)** Average spike waveforms of the sorted units, colored by spatial depth. **(H)** Representative raster plot of all units detected in (G) over a 10-second window.

markedly lower neuroinflammatory response surrounding the Fleuron probe compared to the polyimide control, as evidenced by reduced glial fibrillary acidic protein (GFAP)-positive astrocytes – a widely recognized indicator of brain immune response – which is consistent with our previous findings. We then quantified the accumulation of GFAP expression as a function of the distance to the surface of the probe (**Fig. 3B**). The results indicate that the Fleuron probes exhibit less glial encapsulation at 3-, 6-, and 9- months post-implantation compared to the polyimide control. Additionally, we observed that the GFAP accumulation at the vicinity of the implant is qualitatively more isotropic around the Fleuron probe, while polyimide controls tend to have a more directional GFAP halo, perpendicular to the largest surface of the probe.

We then quantify the size of the cavity surrounding the implanted probes (**Fig. 3C**), which reflects both the acute effects of implantation and the cumulative impact of probe micromotion over time. While cavity sizes were similar across groups at 3 months – corresponding to the acute recovery phase – polyimide controls exhibited substantially larger cavities at 6 and 9 months post-implantation, suggesting progressive tissue disruption and instability compared to the Fleuron probes.

Overall, long-term implantation studies show that Fleuron probes, even at larger dimensions, significantly reduce tissue encapsulation and cavity formation compared to rigid

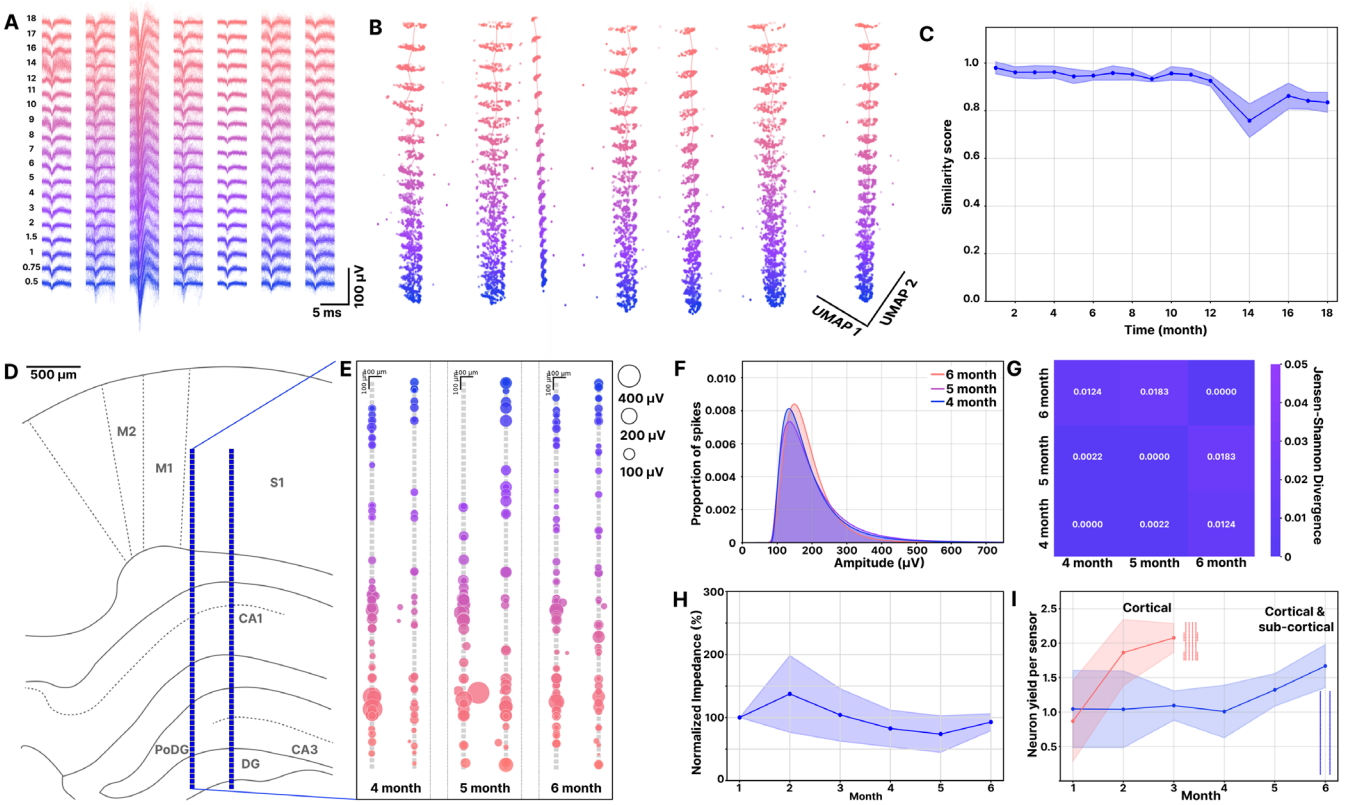

Figure 5 Single-unit level array chronic stability
(A) Overlaid detected waveforms recorded from one-month to eighteen-months post-implantation, recorded by a 500 µm wide Fleuron probe. **(B)** Clusters of detected waveforms in two-dimensional Uniform Manifold Approximation and Projection (UMAP) space recorded from one-month to eighteen-month post-implantation. **(C)** Waveform similarity of detected units. **(D)** Rat brain atlas showing the positioning of the probe across cortical and hippocampal layers. **(E)** Amplitude and centroid distribution of detected neurons at 4-, 5- and 6-month post-implantation, sorted by Kilosort 4. **(F)** Distributions of the spike amplitude over time at 4-, 5- and 6-months post-implantation **(G)** Jensen-Shannon divergence comparison of each distribution from (F) over time. **(H)** Normalized impedance distribution for each channel from 6 implanted devices, relative to the initial value at month 1, as a function of time. Color code: Line = mean; dark blue area = standard deviation. (N = 6 subjects, mean ± standard deviation). **(I)** Average number of neurons detected per electrode (neuron yield) over time (N = 6 subjects, mean ± standard deviation).

polyimide controls. This enhanced biocompatibility enables the integration of a greater number of sensors/stimulators, supporting high-density, tissue-wide, and chronically stable neural interfaces that are difficult to achieve with conventional rigid probes.

Tissue-wide, High-density Recordings

After establishing a new dimensional baseline for chronically stable brain–electronic interfaces using Fleuron probes (**Fig. 3**), we evaluated the stability of neural recordings in a rat model using 450 µm-wide probes (**Fig. 4A**). Each 128-channel Fleuron probe featured 32 × 32 µm² electrode sites, spaced at 40 µm along the insertion axis and either 90 µm or 40 µm laterally between columns, forming six electrode columns in total. This high-density architecture enables multi-site recordings from individual neuronal units within and across columns to optimize spike sorting performances. The multi-column structure is specifically designed to capture tissue-wide, non-redundant and high-density neural activity. To evaluate this capability, the probes were implanted in the primary motor cortex (M1, **Fig. 4B**), allowing high-resolution recording of motor-related brain activity (**Fig. 4D**). Recordings were performed in freely moving rats during naturalistic motor behaviors in real time. Representative voltage traces from a single column highlight the Fleuron probes' ability to achieve high signal-to-noise ratio (SNR) recordings (**Fig. 4E**, and **Fig. 4F**). Rigorous spike sorting using Kilosort 4 (15) revealed that a single Fleuron probe can detect over 100 independent units (**Fig. 4F** and **Fig. 4G**). **Figures 4F and 4H** present the spatial centroids and amplitudes of sorted units (**Fig. 4F**), their average waveform (**Fig. 4G**), and a corresponding raster plot (**Fig. 4H**) of single-unit activity from the recording session, collectively demonstrating the high-density, single-unit-level recording capabilities of Fleuron probes.

Chronically Stable Single- and Multi-unit level Recordings

To evaluate the long-term performance and recording stability of Fleuron probes, we conducted chronic implantation studies extending up to 18 months in freely behaving rodents. In the longest trial, longitudinal overlays of extracellular spike waveforms reveal consistent spike morphology throughout the 18-month period (**Fig. 5A**). High-dimensional spike features projected into a two-dimensional space using Uniform Manifold Approximation and Projection (UMAP), show stable clustering patterns over time (**Fig. 5B**). Additionally, waveform similarity scores across months indicated high pairwise similarity of spike shapes throughout

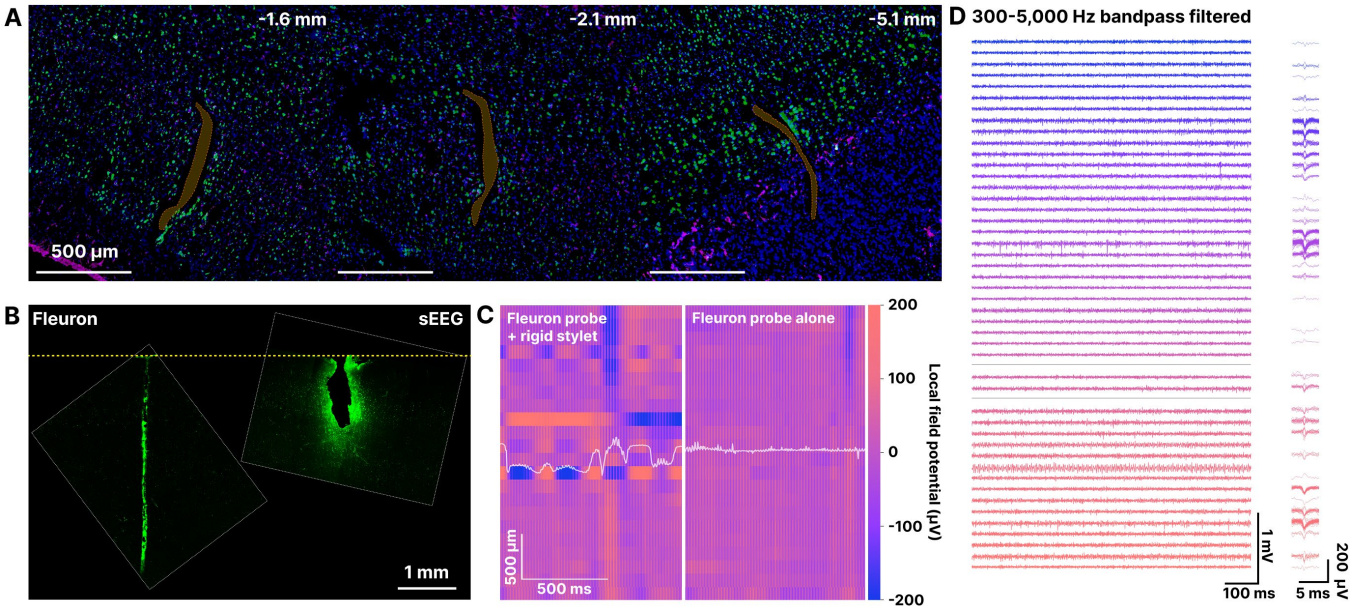

Figure 6. Translation to large animal model and *ex vivo* human tissue.
(A) Representative immunofluorescence images of horizontal brain tissue sections obtained at 2 weeks following implantation of a 700 µm wide, 10 µm thick Fleuron probes in an ovine model. Staining includes DAPI (blue) for cell nuclei, NeuN (green) for neurons, GFAP (pink) for astrocytes indicating glial scarring, and Iba1 (cyan) for activated microglia representing neuroinflammatory responses. Probes' cross-sections are colored in orange. **(B)** Representative fluorescence images of vertical brain *ex vivo* human brain slices after implantation and explanation of a stained Fleuron probe (left) and a stereo-EEG probe (right) as control. The dashed yellow line represents the surface of the human tissue sample from which the probes were implanted. **(C)** Local field potential amplitude as a function of time for the Fleuron probe before (left) and after (right) removal of the stylet. Each row represents a different channel, ordered from top to bottom by depth of implantation The white line represent the estimated motion (scale in µm) of the probe relative to the brain (16). **(D)** (Left) Representative filtered voltage traces during acute recordings in porcine model. (Right) Detected single units during the recording.

the recording period (**Fig. 5C**), suggesting that the same individual neurons or local ensembles were reliably recorded by the same electrode.

To demonstrate the ability of Fleuron probes to capture stable single-unit activity across varying depths, we designed an extended version of the 128-channel probe featuring two electrode columns and implanted it across multiple cortical and hippocampal layers, including S1, CA1, CA3, and DG (**Fig. 5D).** In a representative example we calculated the average waveform amplitude and centroid position of the spike-sorted units using Kilosort 4 at 4, 5, and 6 months post-implantation (**Fig. 5E**), showing that the regions of the array with observed firing activity are similar over time, and that the amplitude distribution of waveform is very consistent across months (**Fig. 5F, G**).

Across the animal cohort (n = 6), normalized electrochemical impedance amplitude at 1 kHz (referenced to values measured one-month post-implantation) remains relatively stable over month two - six (**Fig. 5H**). Notably, we did not observe a drastic drop in impedance over time, which is consistent with bench testing realized on Fleuron probes (12). Additionally, we quantified the average unit yield per electrode across the cohort (**Fig. 5I**) for both array configurations – six-column arrays targeting cortical regions and two-column arrays for deeper brain structures – and found that unit yield generally increased over month one - six, further supporting the long-term stability of Fleuron probes in the brain.

Translation to Large Animals and *Ex Vivo* Human Tissues

To assess the potential of Fleuron probes for clinical translation, we developed longer threads and implantation shuttles (5–10 cm length) suitable for deployment in large animal models and *ex vivo* human brain tissues. In ovine models, histological analysis performed two weeks after implantation of a 700 µm-wide, 10 µm-thick Fleuron probe revealed no evidence of glial encapsulation at different depth (**Fig. 6A**). To evaluate implantation feasibility in human brain tissue, we performed insertions into *ex vivo* specimens using stained Fleuron probes, comparing acute tissue displacement against commercial stereo-EEG electrodes. Longitudinal brain slices (**Fig. 6B**) showed that, upon explantation, Fleuron probes left no residual cavity, in contrast to the stereo-EEG controls, highlighting the minimal invasiveness of the probe and stylet.

Lastly, Fleuron probes were evaluated in a porcine model for intraoperative electrophysiological recordings. Using recently developed methods for high-density laminar arrays (16), we assessed the relative motion of the probe before and after removal of the rigid tungsten stylet. The results show that brain pulsation-induced drift is significantly reduced following stylet removal (**Fig. 6C**), highlighting the mechanical stability of the brain-Fleuron probe interface. We also confirmed the ability of Fleuron probes to reliably capture single-unit activity in large animal models (**Fig. 6D**).

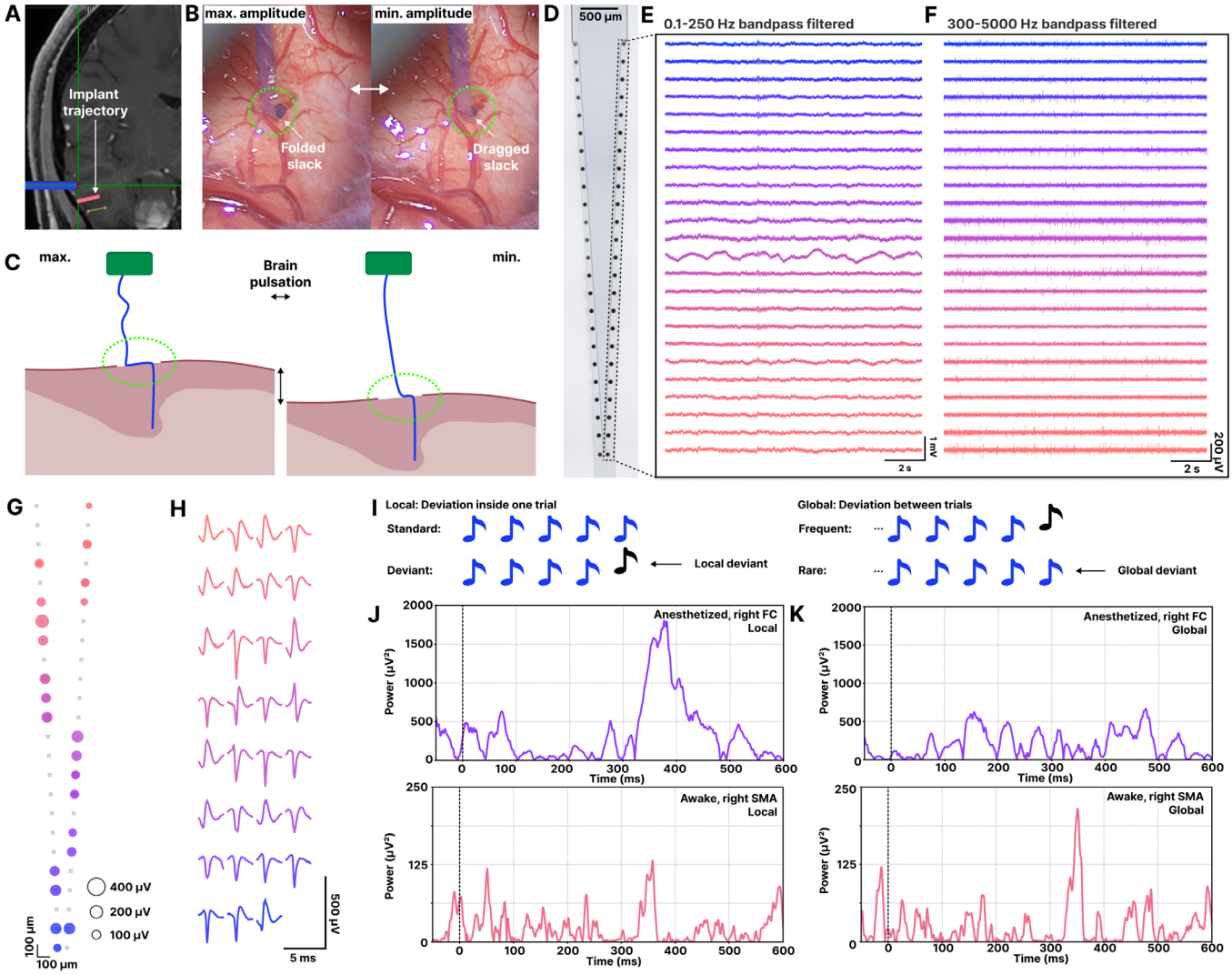

Figure 7. Acute neural recordings using Fleuron probes in human cortex.
(A) Pre-operative MRI overlaid with the planned implantation trajectory following neuronavigation calibration. **(B)** Intraoperative photographs of a Fleuron probe (colored in blue) on human cortical surface during the cardiac cycle, showing the probe slack displacement between the maximum and minimum of amplitude of brain movement. **(C)** Schematic representation of probe motion induced by the cyclic brain movement. **(D)** Microscopic image of the implanted Fleuron probe, **(E)** Raw and **(F)** 300-5,000 Hz band-pass filtered neural signals acquired from each channel shortly after insertion. **(G)** Visualization of spike sorting results using Kilosort 4, showing the spatial distribution (centroid) and relative amplitude of identified units across the probe's channels. **(H)** Average spike waveforms of the sorted units, colored by spatial depth. **(I)** Schematic illustration of local and global deviance paradigms using auditory stimuli. (Left) Local deviance refers to a deviation within a single trial. The deviant sequence ends with a different tone (pink), compared to the standard sequence where all tones are identical (blue). (Right) Global deviance reflects a deviation across trials. The globally rare sequence (top) differs in pattern from the frequent one, despite having the same local structure, thereby creating a global deviant. **(J)** Difference in averaged LFP power over time recorded from the right frontal cortex of an anesthetized patient, and **(K)** from the right supplementary motor area (SMA) of an awake patient, in response to an auditory local deviant (upper panels) and a global deviant (lower panels).

Intra-operative Recordings in Humans

We conducted intra-operative neural recordings in human patients undergoing resection surgery, to demonstrate that the implantation and explantation techniques developed in large animal models are directly translatable to clinical settings. Implantation trajectory was determined using standard neuronavigation and MRI pre-operative imaging (**Fig. 7A**). Following implantation at approximately 1 cm depth in the cortex, we observe that the Fleuron probe coupled with the natural motion of the brain due to its compliance and the presence of slack between the implantation site and the headstage (**Fig. 7B-D**). Representative and filtered voltage traces from the probe (**Fig. 7E, F**) show the detection of both local field potentials and stable spikes from the onset of implantation in the brain and throughout the entire recording window (20 mins). Spike sorting shows that a mixture of somatic and non-somatic single units can be detected along the entire length of the probe with electrodes (**Fig. 7G, H**).

Finally, we perform an auditory local-global deviant paradigm (17) in both anesthetized and awake patients (**Fig. 7I**). In an anesthetized patient, we show that a peak in the local field potential power is observed approximately 350 ms after the start of the local deviant tone. However, no qualitative peak is observed after a global deviant (**Fig. 7J**), which is expected

from the depth of unconsciousness caused by the anesthesia. In an awake patient, the same auditory paradigm was conducted, revealing a clear peak in local field potential power following both the local and global deviants, occurring approximately 350 ms after the onset of the deviant tone (**Fig. 7K**), which is consistent with neural signatures expected in a conscious state. These observations are in line with previous studies (17). Overall, this experiment highlights the potential of high-resolution cortical laminar electrophysiology to rapidly detect both sensory-evoked potentials and neural correlates of conscious processing, enabling the evaluation of consciousness states with high signal-to-noise ratio and temporal precision.

Conclusion

In this work, we demonstrate that ultrasoft Fleuron probes enable stable, high-density brain–computer interfaces, effectively overcoming the long-standing trade-off between recording density and chronic stability inherent to rigid materials like polyimide or silicon. We show that Fleuron probes can be integrated in iBCI systems with low-power, mixed-signal and bidirectional ASIC, and deployed at depth in the brain using established, minimally invasive neurosurgical techniques. Importantly, Fleuron probes were used for the first time in humans to record stable, high-resolution single-unit activity at depth within the brain, including evoked responses to auditory oddball paradigms to measure neural correlates of consciousness – underscoring the readiness of this technology for clinical translation.

Ethical Considerations

All experiments involving animals were conducted in accordance with institutional and federal guidelines, and regulations for the care and use of laboratory animals.

All rodent procedures were approved by the Institutional Animal Care and Use Committee (IACUC) at Mispro Biotech, Cambridge, MA (Protocol No. 2022-AXO-01).

All porcine procedures were approved by the Institutional Animal Care and Use Committee (IACUC) at the Massachusetts General Hospital, Boston, MA (Protocol No. 2010N000198).

All ovine procedures were approved by the Institutional Animal Care and Use Committee (IACUC) at Tufts Comparative Medicine-Preclinical Services, Boston, MA (Protocol No. B2023-71).

All *ex vivo* human tissue procedures were authorized by the University Health Network Research Ethics Board.

The study involving human participants was approved by the Ethics Committee at The Panama Clinic, registered under ClinicalTrials.gov ID NCT06673264. Participants were scheduled to undergo a planned surgery for brain tissue resection of either a tumor or of an epileptogenic lesion. The Axoft device was implanted into normal brain tissue scheduled for surgical resection. All participants provided written informed consent prior to participation.

Acknowledgements

We thank all the clinical study participants, clinical and non-clinical team members, for being involved in this work. Human subject research was conducted at The Panama Clinic with clinical study development done in collaboration with Bioaccess®. The porcine study was supported by NIH NICHD R01 HD099397 to BCB[e].

Author contributions

Conceptualization: PLF, TY, JL[a], JL[a,b]. All authors from Axoft, Inc. contributed to experimental design, data analysis, and manuscript preparation. ACP[d], BC[d], SSC[d], BCB[e], BB[e], TS[e] lead and organized the porcine study. HMC[f], MM[f], BB[g], DZ[h], TAV[f, i] lead and organized the *ex vivo* human tissue study. RB[j] was the Principal Investigator for the clinical study. RB[j], AF[j] and CC[j] performed the surgeries during the clinical study.

Competing interest statement

This research was funded and supported by Axoft, Inc.

Data availability statement

Sample datasets in the present study are available upon reasonable request to the authors.

References

1 J.D. Steinmetz, K.M. Seeher, N. Schiess, E. Nichols, B. Cao, C. Servili, V., Cousin Cavallera, E., H. Hagins, M.E. Moberg and M.L. Mehlman, Global, regional, and national burden of disorders affecting the nervous system, 1990–2021: a systematic analysis for the Global Burden of Disease Study 2021. The Lancet Neurology, 23(4), 344-381 (2024).

2. F. R. Willett, E. M. Kunz, C. Fan, D. T. Avansino, G. H. Wilson, E. Y. Choi, F. Kamdar, M. F. Glasser, L. R. Hochberg, S. Druckmann, K. V Shenoy, J. M. Henderson, A high-performance speech neuroprosthesis. Nature 620, 1031–1036 (2023).

3. S. L. Metzger, K. T. Littlejohn, A. B. Silva, D. A. Moses, M. P. Seaton, R. Wang, M. E. Dougherty, J. R. Liu, P. Wu, M. A. Berger, I. Zhuravleva, A. Tu-Chan, K. Ganguly, G. K. Anumanchipalli, E. F. Chang, A high-performance neuroprosthesis for speech decoding and avatar control. Nature 620, 1037–1046 (2023).

4. N. A. Steinmetz, C. Aydin, A. Lebedeva, M. Okun, M. Pachitariu, M. Bauza, M. Beau, J. Bhagat, C. Böhm, M. Broux, S. Chen, J. Colonell, R. J. Gardner, B. Karsh, F. Kloosterman, D. Kostadinov, C. Mora-Lopez, J. O'Callaghan, J. Park, J. Putzeys, B. Sauerbrei, R. J. J. van Daal, A. Z. Vollan, S. Wang, M. Welkenhuysen, Z. Ye, J. T. Dudman, B. Dutta, A. W. Hantman, K. D. Harris, A. K. Lee, E. I. Moser, J. O'Keefe, A. Renart, K. Svoboda, M. Häusser, S. Haesler, M. Carandini, T. D. Harris, Neuropixels 2.0: A miniaturized high-density probe for stable, long-term brain recordings. Science 372, eabf4588 (2021).

5. M. Azabou, V. Arora, V. Ganesh, X. Mao, S. Nachimuthu, M. J. Mendelson, B. Richards, M. G. Perich, G. Lajoie, E. L. Dyer, A Unified, Scalable Framework for Neural Population Decoding. (2023).

6. M. Safaie, J.C. Chang, J. Park, L.E. Miller, J.T. Dudman, M.G. Perich and J.A. Gallego. Preserved neural dynamics across

animals performing similar behaviour. Nature, 623(7988), 765-771 (2023).

7. J. W. Salatino, K. A. Ludwig, T. D. Y. Kozai, E. K. Purcell, Glial responses to implanted electrodes in the brain. Nat. Biomed. Eng. 1, 862–877 (2017).

8. A. C. Paulk, Y. Kfir, A. R. Khanna, M. L. Mustroph, E. M. Trautmann, D. J. Soper, S. D. Stavisky, M. Welkenhuysen, B. Dutta, K. V. Shenoy, L. R. Hochberg, R. M. Richardson, Z. M. Williams, S. S. Cash, Large-scale neural recordings with single neuron resolution using Neuropixels probes in human cortex. Nat. Neurosci. 25, 252–263 (2022).

9. Y. He, A. Marin-Llobet, H. Sheng, R. Liu, J. Liu, End-to-end multimodal deep learning for real-time decoding of months-long neural activity from the same cells. bioRxiv, 2024.10.14.618046 (2024).

10. E. Musk. An integrated brain-machine interface platform with thousands of channels. Journal of medical Internet research, 21(10), p.e16194 (2019).

11. F. Vashahi, H. Park, X. Gong, A. Parekh, J. Liu, T. Ye, P. Le Floch, Soft, Biocompatible and High-Performance Photo-Patternable Dielectrics for High-Density and Chronically Stable Brain-Electrode Interfaces, 2024 IEEE International Electron Devices Meeting (IEDM), 1–4 (2024).

12. P. Le Floch, S. Zhao, R. Liu, N. Molinari, E. Medina, H. Shen, Z. Wang, J. Kim, H. Sheng, S. Partarrieu, W. Wang, C. Sessler, G. Zhang, H. Park, X. Gong, A. Spencer, J. Lee, T. Ye, X. Tang, X. Wang, K. Bertoldi, N. Lu, B. Kozinsky, Z. Suo, J. Liu, 3D spatiotemporally scalable in vivo neural probes based on fluorinated elastomers. Nat. Nanotechnol. 19, 319–329 (2024).

13. A. Fornito, A. Zalesky and M. Breakspear. The connectomics of brain disorders. Nat. Rev. Neurosci. *16*(3), 159-172 (2015).

14. A.V. Ulyanova, C. Cottone, C.D. Adam, K.G. Gagnon, D.K. Cullen, T. Holtzman, B.G. Jamieson, P.F. Koch, H.I. Chen, V.E. Johnson and J.A. Wolf. Multichannel silicon probes for awake hippocampal recordings in large animals. Front. Neurosci. *13*, 397 (2019).

15. M. Pachitariu, S. Sridhar, J. Pennington, C. Stringer, Spike sorting with Kilosort4. Nat Methods 21, 914–921 (2024).

16. C. Windolf, H. Yu, A. C. Paulk, D. Meszéna, W. Muñoz, J. Boussard, R. Hardstone, I. Caprara, M. Jamali, Y. Kfir, D. Xu, J. E. Chung, K. K. Sellers, Z. Ye, J. Shaker, A. Lebedeva, M. Raghavan, E. Trautmann, M. Melin, J. Couto, S. Garcia, B. Coughlin, C. Horváth, R. Fiáth, I. Ulbert, J. A. Movshon, M. N. Shadlen, M. M. Churchland, A. K. Churchland, N. A. Steinmetz, E. F. Chang, J. S. Schweitzer, Z. M. Williams, S. S. Cash, L. Paninski, and E. Varol. DREDge: robust motion correction for high-density extracellular recordings across species. Nat. methods, 1-13 (2025).

17. T. A. Bekinschtein, S. Dehaene, B. Rohaut, F. Tadel, L. Cohen, L. Naccache, Neural signature of the conscious processing of auditory regularities. Proc. Natl. Acad. Sci. U.S.A. 106, 1672–1677 (2009).

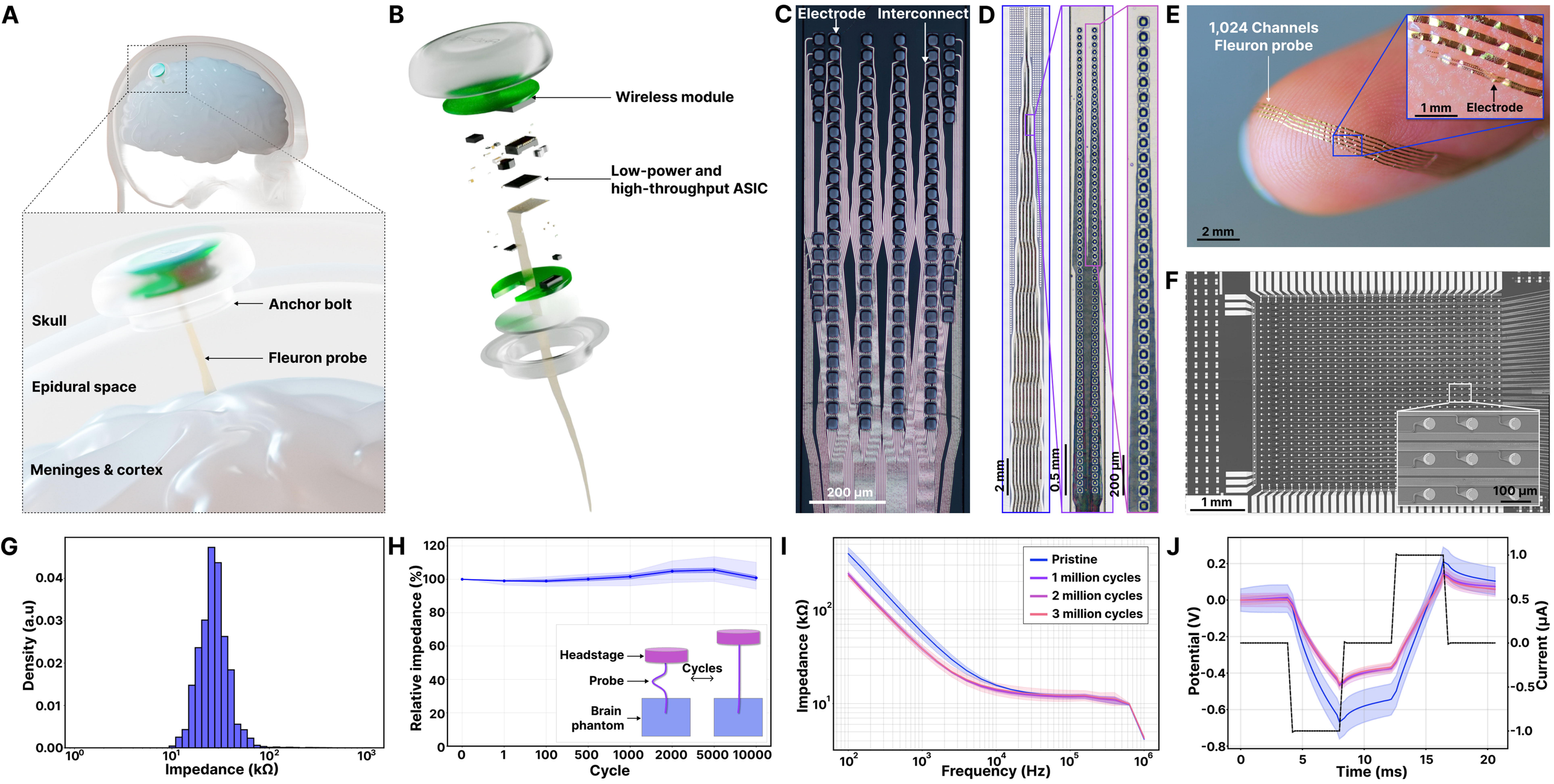
A
Anchor bolt
Skull
Fleuron probe
Epidural space
Meninges & cortex
B
Wireless module
Low-power and
high-throughput ASIC
C
Electrode
Interconnect
200 µm
D
2 mm
0.5 mm
200 µm
E
1,024 Channels
Fleuron probe
1 mm
Electrode
2 mm
F
1 mm
100 µm
G
Density (a.u)
Impedance (kΩ)
H
Relative impedance (%)
Cycle
Headstage
Probe
Brain
phantom
Cycles
I
Impedance (kΩ)
Frequency (Hz)
Pristine
1 million cycles
2 million cycles
3 million cycles
J
Potential (V)
Current (µA)
Time (ms)

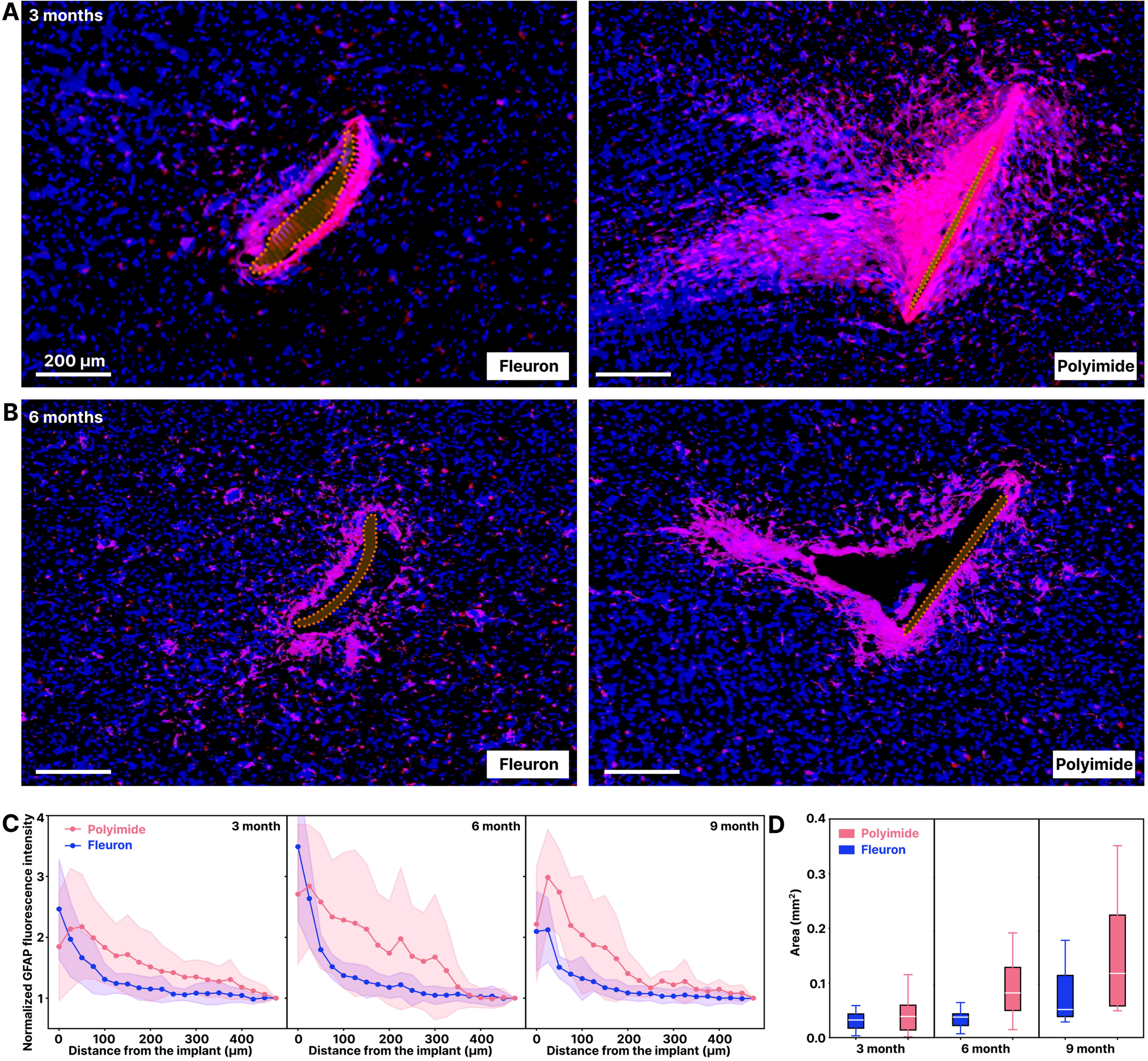
A
3 months
200 µm
Fleuron
Polyimide
B
6 months
Fleuron
Polyimide
C
Polyimide
Fleuron
3 month
6 month
9 month
Normalized GFAP fluorescence intensity
Distance from the implant (µm)
D
Polyimide
Fleuron
Area (mm²)
3 month
6 month
9 month

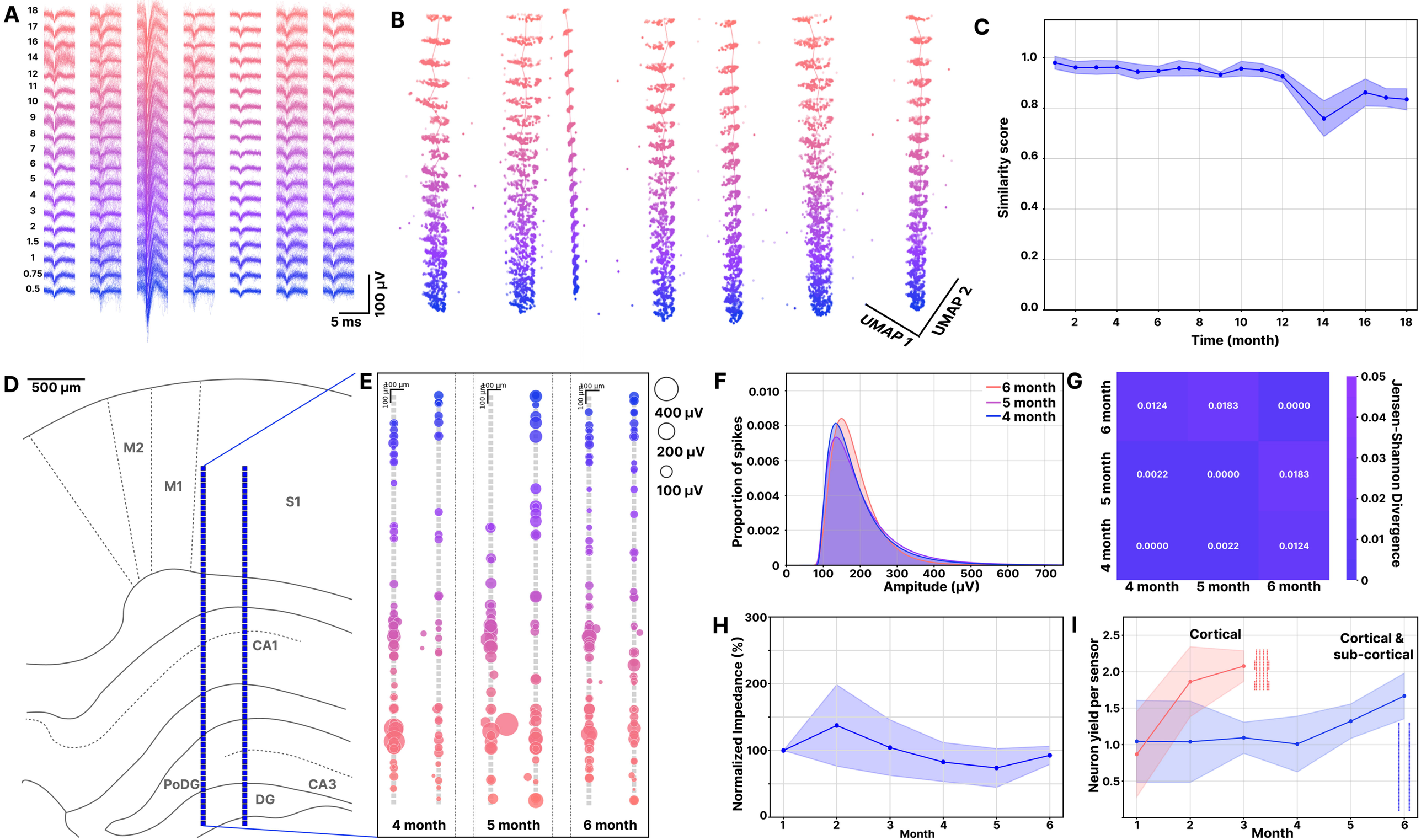
A
18
17
16
14
12
11
10
9
8
7
6
5
4
3
2
1.5
1
0.75
0.5
100 µV
5 ms
B
UMAP 1
UMAP 2
C
Similarity score
Time (month)
D
500 µm
M2
M1
S1
CA1
PoDG
DG
CA3
E
100 µm
400 µV
200 µV
100 µV
4 month
5 month
6 month
F
6 month
5 month
4 month
Proportion of spikes
Amplitude (µV)
G
6 month
5 month
4 month
0.0124
0.0183
0.0000
0.0022
0.0000
0.0183
0.0000
0.0022
0.0124
Jensen-Shannon Divergence
H
Normalized Impedance (%)
Month
I
Cortical
Cortical &
sub-cortical
Neuron yield per sensor
Month

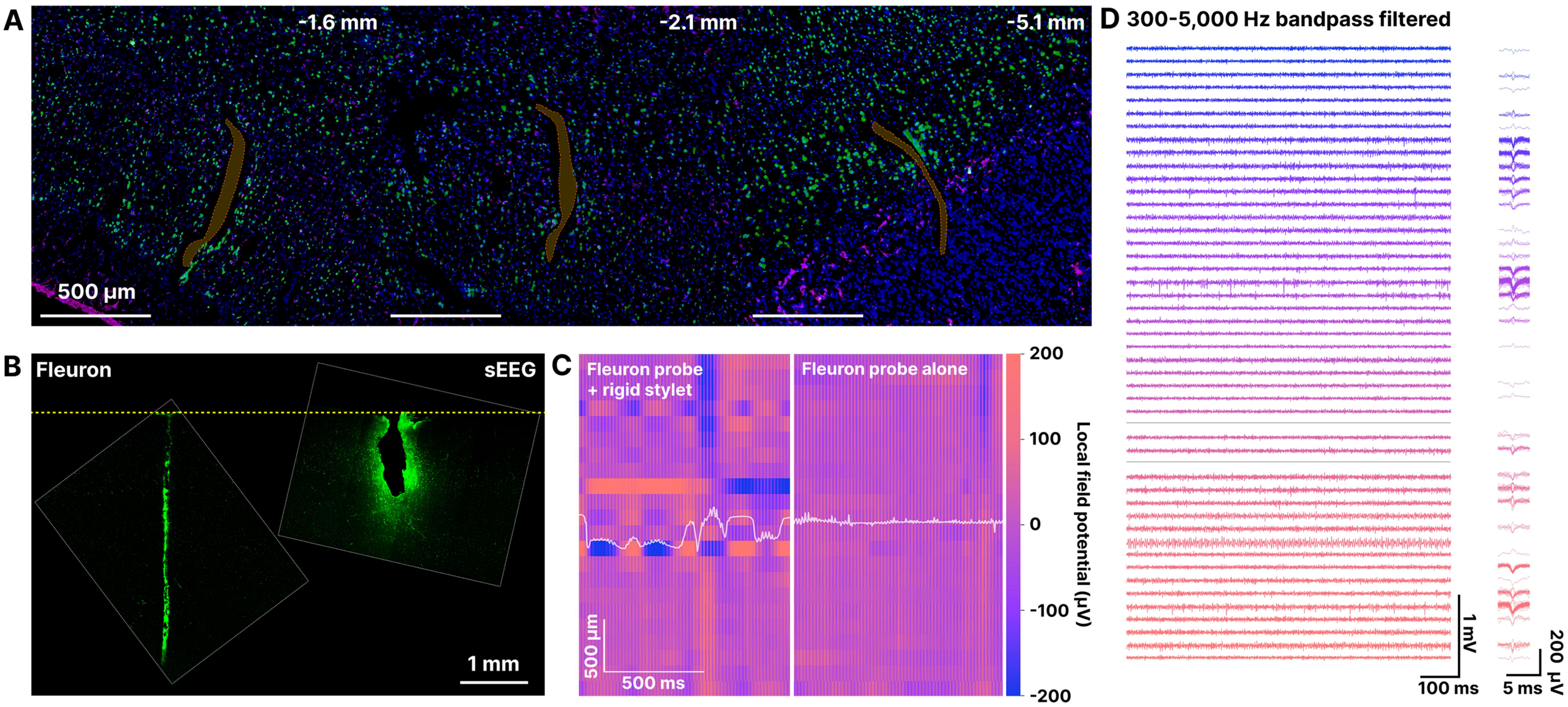
A
-1.6 mm
-2.1 mm
-5.1 mm
500 µm
B
Fleuron
sEEG
1 mm
C
Fleuron probe
+ rigid stylet
Fleuron probe alone
500 µm
500 ms
200
100
0
-100
-200
Local field potential (µV)
D
300-5,000 Hz bandpass filtered
1 mV
100 ms
200 µV
5 ms

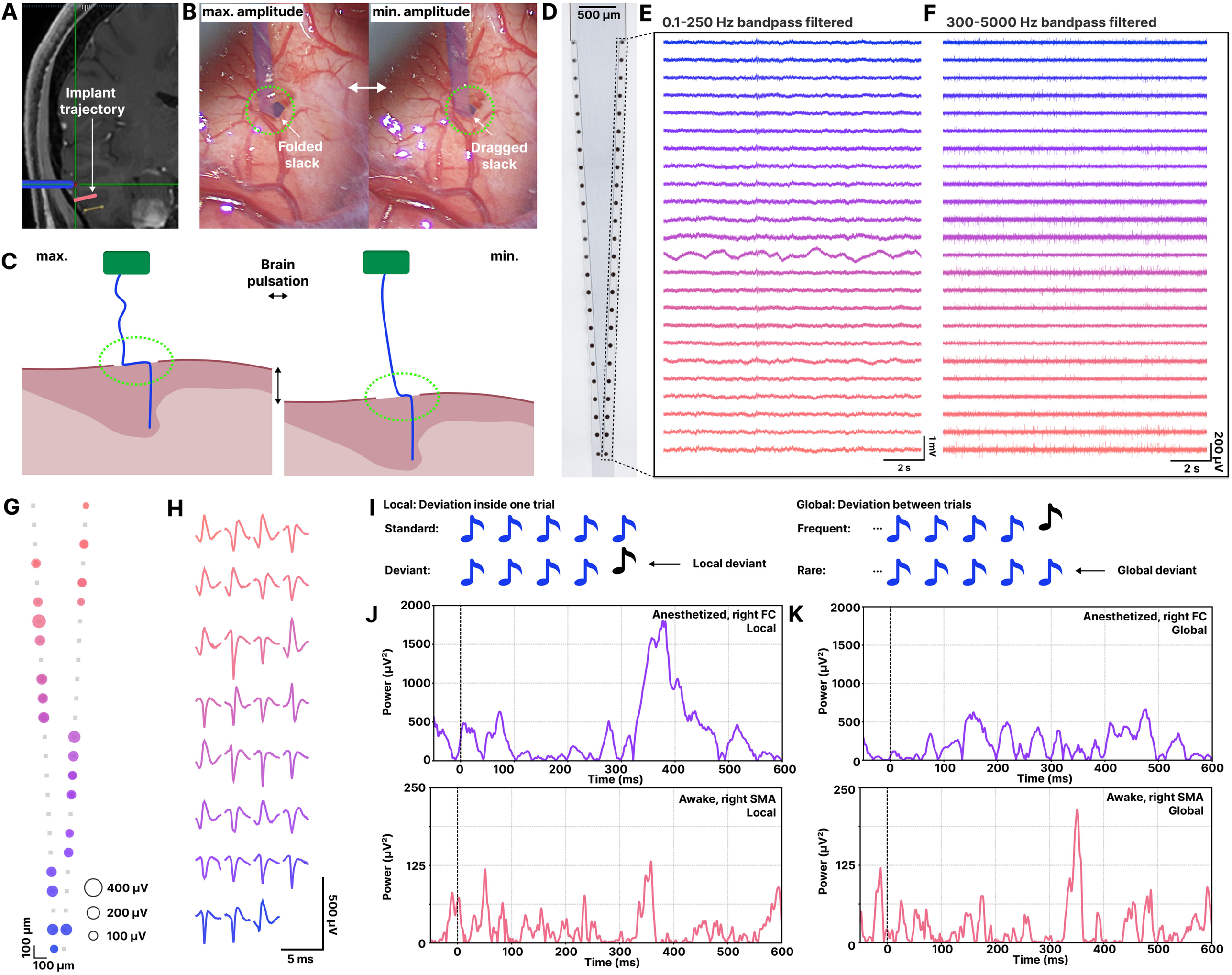
A
Implant trajectory
B
max. amplitude
min. amplitude
Folded slack
Dragged slack
C
max.
Brain pulsation
min.
D
500 µm
E
0.1-250 Hz bandpass filtered
F
300-5000 Hz bandpass filtered
1 mV
2 s
200 µV
2 s
G
400 µV
200 µV
100 µV
100 µm
100 µm
H
500 µV
5 ms
I
Local: Deviation inside one trial
Standard:
Deviant:
Local deviant
Global: Deviation between trials
Frequent:
Rare:
Global deviant
J
Anesthetized, right FC
Local
Awake, right SMA
Local
Power (µV²)
Time (ms)
K
Anesthetized, right FC
Global
Awake, right SMA
Global
Power (µV²)
Time (ms)

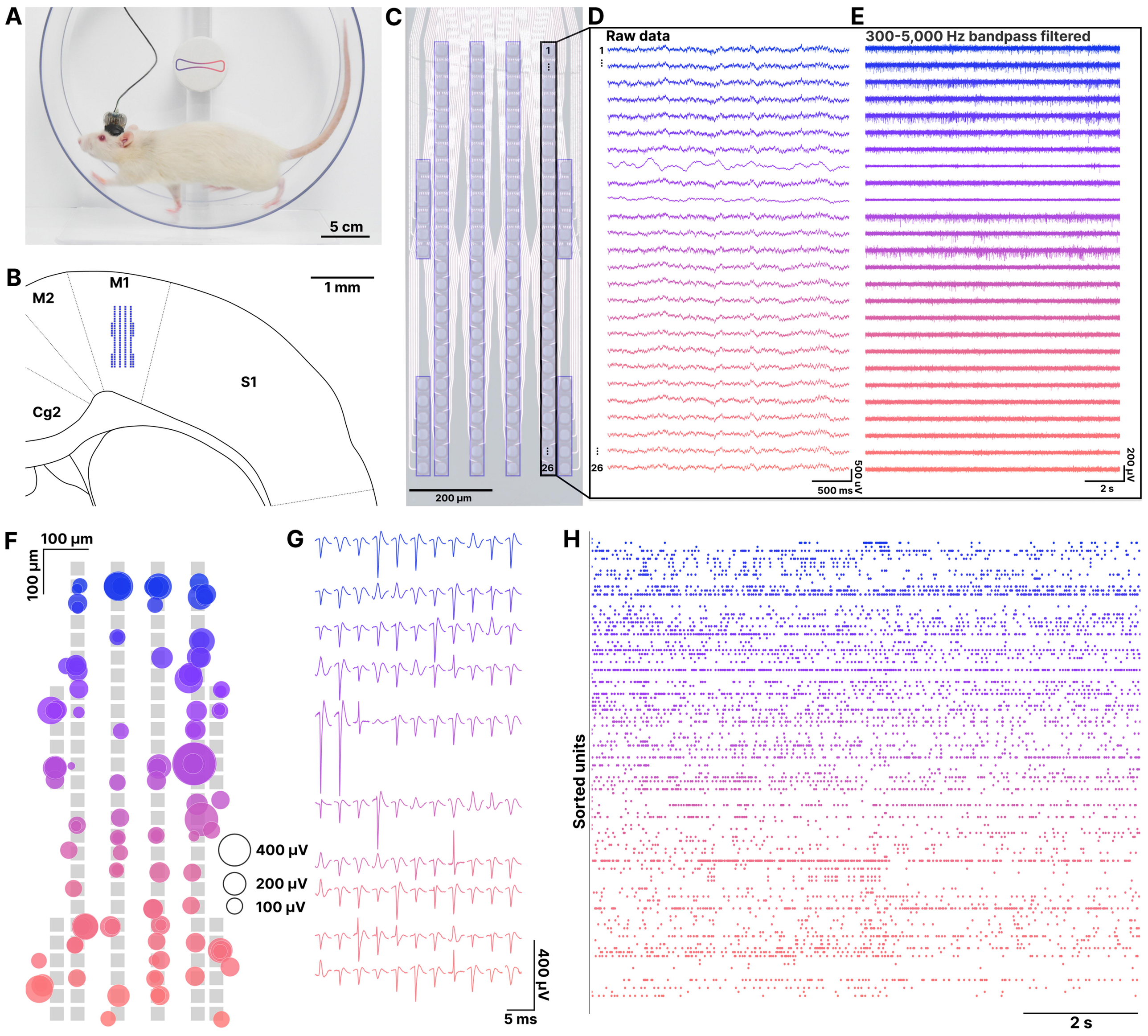
A
5 cm
B
M2
M1
1 mm
S1
Cg2
C
1
26
200 µm
D
Raw data
1
26
500 µV
500 ms
E
300-5,000 Hz bandpass filtered
200 µV
2 s
F
100 µm
100 µm
400 µV
200 µV
100 µV
G
400 µV
5 ms
H
Sorted units
2 s

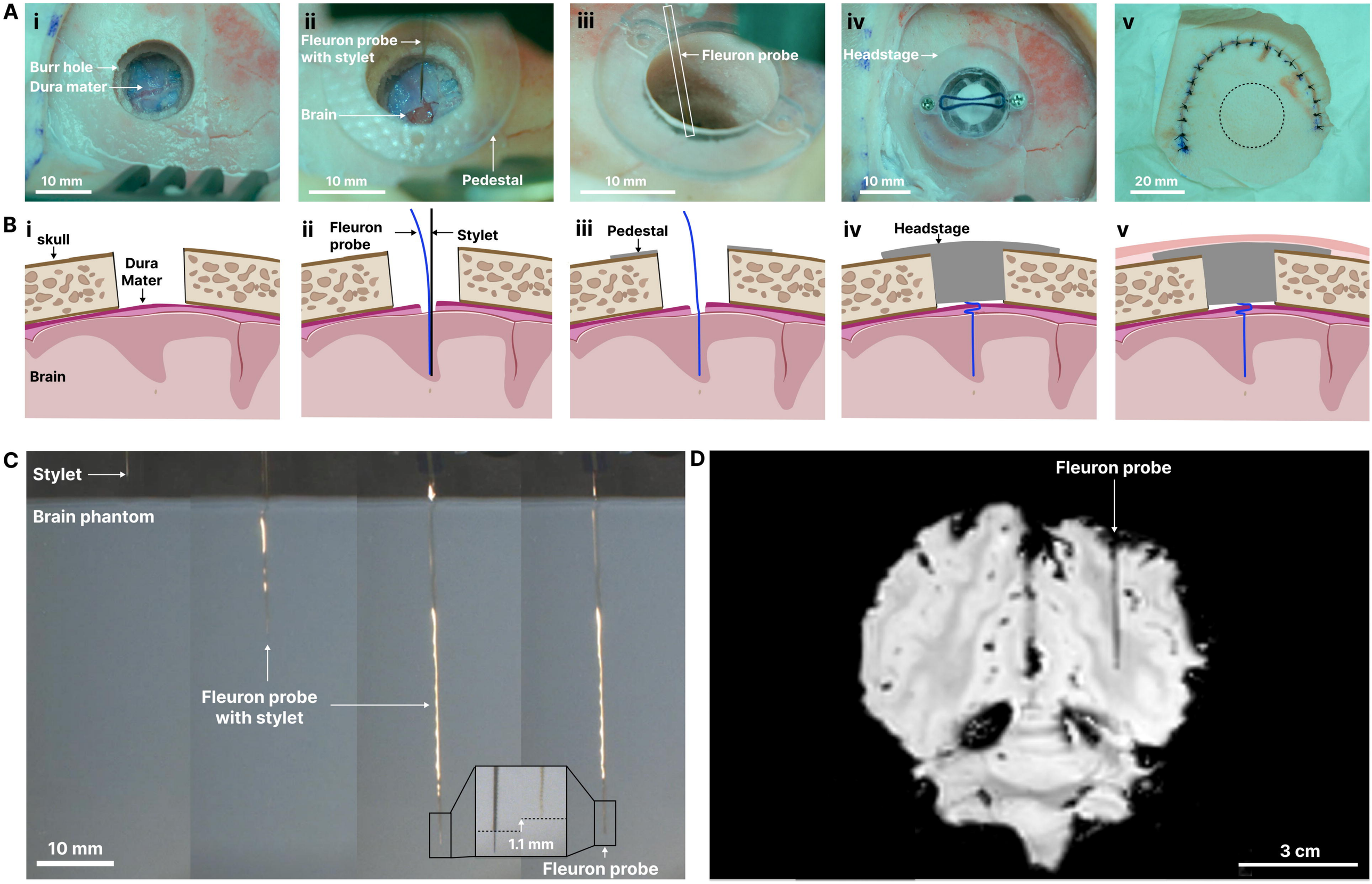
A
i
Burr hole
Dura mater
10 mm
ii
Fleuron probe with stylet
Brain
Pedestal
10 mm
iii
Fleuron probe
10 mm
iv
Headstage
10 mm
v
20 mm
B
i
skull
Dura Mater
Brain
ii
Fleuron probe
Stylet
iii
Pedestal
iv
Headstage
v
C
Stylet
Brain phantom
Fleuron probe with stylet
1.1 mm
Fleuron probe
10 mm
D
Fleuron probe
3 cm